Performance Analysis of Scarfed Nozzles

Jay S. Lilley*
U.S. Army Missile Command, Redstone Arsenal, Alabama
and
Joe D. Hoffman†
Purdue University, West Lafayette, Indiana

An analysis for predicting the performance of side-exhausting scarfed propulsive nozzles is presented. Nozzles of this type consist of a conventional axisymmetric nozzle followed by a scarfed conical extension. They are employed in situations where the exhaust jet must exit through the side of a missile. The flowfield model assumes that the flow within the nozzle is axisymmetric, and that the overall nozzle pressure ratio is high enough to preclude shock waves or flow separation at the nozzle exit. The flowfield is calculated by the method of characteristics. The oblique shock wave that emanates from the junction of the nozzle and the nozzle extension is fitted discretely and tracked through the flowfield. The forces and moments acting on the scarfed nozzle and the missile are determined. The results of an extensive parametric study are presented. Comparisons with experimental measurements are presented to verify the analysis.

Nomenclature

F = thrust
$\dot{m}$ = mass flow rate
P = static pressure
P_a = atmospheric pressure
X, Y = missile coordinates
x, y = nozzle coordinates
α = nozzle cone angle
β = nozzle scarf angle
γ = specific heat ratio
δ = scarfed extension cone angle
ϵ = nozzle area ratio
η = nozzle thrust efficiency
θ = nozzle cant angle

Introduction

THE conventional propulsive nozzle is an axisymmetric converging-diverging nozzle terminating in a plane perpendicular to the axis of the nozzle. If the flow entering the nozzle is axisymmetric, then the flow in the nozzle is also axisymmetric, and the resultant thrust vector lies along the nozzle axis.

In applications where the nozzle exits through the side of a missile, the nozzle axis is canted with respect to the missile axis. If the nozzle terminates along the line of intersection of the nozzle contour and the missile outer skin, the nozzle is scarfed. If the nozzle exit is flush with the missile skin, which is usually the case, then the nozzle cant angle and the nozzle scarf angle are the same. Figure 1 illustrates such a canted scarfed propulsive nozzle.

The plume from a scarfed nozzle is always three-dimensional. However, when the Mach angle along the exit lip of a scarfed nozzle is less than the scarf angle, the three-dimensional flow effects do not propagate into the internal flowfield, and the internal flowfield remains axisymmetric. Such is the case considered in the present investigation. Even when the Mach angle is somewhat larger than the scarf angle, only a very small portion of the internal flowfield is influenced by three-dimensional flow effects, and the axisymmetric model is still quite accurate.

In the present study,[1] an axisymmetric flow model is presented for predicting the performance of canted scarfed propulsive nozzles. An extensive parametric study is presented to identify the effects of the various nozzle geometric parameters on missile axial thrust. Comparisons with the results of several experimental programs are presented to verify the performance prediction model.

Nozzle Geometric Model

Figure 2 presents a meridional plane view of the geometric model. The basic nozzle consists of a double circular-arc throat contour joined smoothly to a supersonic expansion contour, which can be conical or contoured. The nozzle extension consists of a conical section beginning at the end of the basic nozzle, point E, and ending at point F. The cant angle θ is the angle in the meridional plane between the nozzle and missile axes. In the present analysis, the cant angle θ is equal to the nozzle scarf angle β.

The throat geometry is completely specified by the throat radius y_t, the throat upstream and downstream radii of curvature ρ_{tu} and ρ_{td}, respectively, and the throat attachment angle θ_a, where the supersonic expansion contour attaches smoothly to the circular-arc throat contour. The geometry of the nozzle extension is completely specified by the location of the attachment point, point E, the angle δ of the conical extension, and the scarf angle β.

If the nozzle extension attaches smoothly to the basic nozzle (i.e., $\theta_e = \delta$), then a continuous flow occurs across the transition region. If δ is less than θ_e, then an oblique shock wave

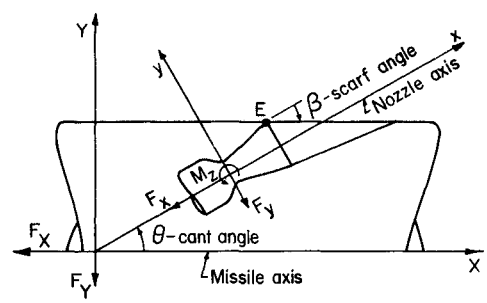

Fig. 1 Side-exiting canted scarfed propulsive nozzle.

Presented as Paper 84-1416 at the AIAA/SAE/ASME 20th Joint Propulsion Conference, Cincinnati, OH, June 11-13, 1984; submitted Aug. 14, 1984; revision received May 29, 1985. This paper is declared a work of the U.S. Government and therefore is in the public domain.

*Aerospace Engineer, Propulsion Directorate. Member AIAA.
†Professor of Mechanical Engineering, Thermal Sciences and Propulsion Center. Member AIAA.

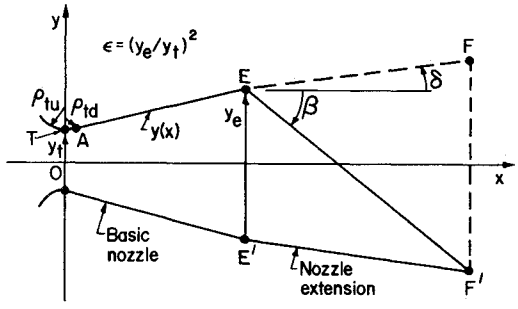

Fig. 2 Scarfed nozzle geometric model.

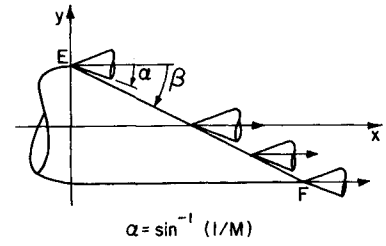

Fig. 3 Side view of scarfed nozzle.

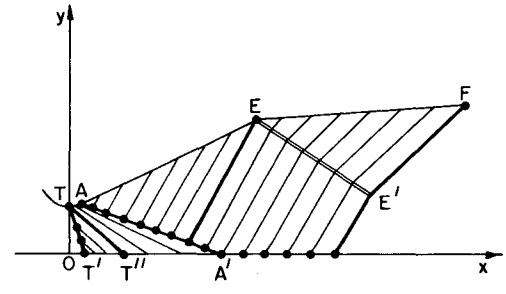

Fig. 4 Overall features of the flowfield.

emanates from point E and propagates downstream into the nozzle extension. Both possibilities are accounted for in the present analysis.

Flowfield Model

The analysis is based on the assumption that the flowfield within the scarfed nozzle extension is axisymmetric. That is the case when the Mach angle along the exit lip of the scarfed nozzle extension is less than the scarf angle. This situation is illustrated best by the side view of a scarfed nozzle extension presented in Fig. 3. In this view, the scarfing plane is perpendicular to the xy plane. If the Mach angle α is less than the scarf angle β, then the Mach cones emanating from the exit lip propagate downsteam of the scarfing plane, and the influence of the flowfield at a given point on the exit lip cannot propagate inside the scarfed extension. However, even for modest amounts of three-dimensional internal flow penetration, the bulk of the flowfield within the scarfed extension remains axisymmetric. Based on these considerations, the flowfield in the scarfed extension is modeled as an axisymmetric flowfield.

The axisymmetric flowfield model consists of four major parts: 1) steady axisymmetric transonic potential flow in the nozzle throat region, 2) steady axisymmetric supersonic irrotational flow in the basic nozzle, 3) flow across an oblique shock wave, and 4) steady axisymmetric supersonic rotational flow in the scarfed extension.

The flow is assumed to originate upstream of the nozzle in a uniform flow region having constant stagnation pressure and temperature, P_t and T_t, respectively. The flowing fluid is assumed to be a thermally and calorically perfect gas (i.e., constant molecular weight and specific heats). The presence of condensed phases is neglected, thus the model applies to clean gas flows or flows having only a small amount of condensed phases. Chemical reactions are neglected, and boundary-layer effects are considered negligible. Consequently, the flowfield is isentropic everywhere except across the oblique shock wave. The flowfield in the transonic region and in the basic nozzle is irrotational (i.e., constant entropy and stagnation enthalpy throughout) since the flow originates in a uniform flow region and is isentropic. The flowfield downstream of the oblique shock wave is rotational due to the transverse entropy gradient produced by the curved oblique shock wave.

The numerical procedure developed in the present investigation is based on the method of characteristics. Essentially, the method of characteristics is a coordinate transformation in which the computational coordinates (i.e., the streamlines and Mach lines) are also the paths of propagation of information through the flowfield. This close matching of the numerical propagation paths and the physical propagation paths results in an extremely accurate modeling of the flowfield.

The overall features of the flowfield are illustrated in Fig. 4. A supersonic initial-value line is constructed across the nozzle throat region using the transonic flow analysis developed by Kliegel and Levine.[2] The method of characteristics for steady two-dimensional supersonic flow, as described by Zucrow and Hoffman,[3] is employed to construct a network of Mach lines in the nozzle and the scarfed extension, on which the flowfield properties are determined. Right-running Mach lines are initiated from points on the initial-value line and from points along the nozzle throat contour TA. Left-running Mach lines are initiated from points along right-running Mach line AA′ until point E is located. Right-running oblique shock wave EE′ emanates from point E. The flowfields in the nozzle and the scarfed extension are patched together across the shock wave EE′. After the entire nozzle flowfield has been calculated, the performance of the scarfed nozzle can be computed.

Performance Model

The performance of a propulsive nozzle is specified by its mass flow rate, thrust vector, and moment vector. For conventional nozzles, the thrust vector lies along the nozzle axis, and the only thrust component is the axial component. In that case, all of the moments are zero. For a scarfed nozzle, side forces and moments are present. The present section presents the performance model for the scarfed nozzle configurations considered in this study.

The nozzle mass flow rate $\dot{m}$, discharge coefficient C_D, and initial-value line thrust F_{IVL} are obtained by numerical integration across line TT′. The thrust F_{SS} developed by the supersonic portion of the nozzle is obtained by integrating (numerically) the axial component of the force developed by the pressure acting on the wall contour TE.

It is assumed that the scarfed extension is axisymmetric (in fact, conical) and that the exit of the scarfed extension is scarfed by a plane perpendicular to the xy plane, which passes through point E on the top of the nozzle where scarfing begins and through point F on the bottom of the nozzle where scarfing ends. Consequently, the flowfield is symmetrical about the xy plane. Thus, as illustrated in Fig. 1, only two force components exist for the scarfed extension, $F_{x,E}$ and $F_{y,E}$, and only one moment component exists, M_z. The force components and the moment are assumed to act at the center of the nozzle throat. The thrust and moment developed by the scarfed extension are obtained by integrating (numerically) the differential force and moment components developed by the pressure acting on the wall of the scarfed extension.

The total axial force F_x acting on the scarfed nozzle is

$$F_x = F_{IVL} + F_{SS} + F_{x,E} \tag{1}$$

The side force F_y acting on the scarfed nozzle is simply $F_{y,E}$. The scarfed nozzle axial specific impulse is given by

$$I_{sp,x} = F_x/\dot{m} \tag{2}$$

The geometric relationship between the nozzle and missile axes is illustrated in Fig. 1. The missile coordinate system is denoted by XY. The nozzle coordinate system xy is assumed to lie in the meridional plane through the missile axis, i.e., in the XYY plane. The forces F_X and F_Y acting on the missile are

$$F_X = F_x\cos\beta - F_y\sin\beta \tag{3}$$

$$F_Y = F_x\sin\beta + F_y\cos\beta \tag{4}$$

The missile axial specific impulse is given by

$$I_{sp,X} = F_X/\dot{m} \tag{5}$$

In the present analysis, the major item of interst is the axial thrust F_X delivered by the rocket motor to the missile. It is assumed that several rocket motors (at least two) are arranged symmetrically around the circumference of the missile, so that all side forces and moments exactly cancel. If this is not the case, the analysis may be easily extended to determine the moments associated with the scarfed nozzle.

Effect of Nozzle Pressure Ratio

From Fig. 1, it is obvious that the scarfed nozzle exit flow area lies on the missile skin. Consequently, the pressure forces acting on that area are normal to the missile axis and do not have any components in the missile axial direction. Thus, the missile axial thrust is independent of the atmospheric pressure. The missile axial thrust and nozzle mass flow rate both depend linearly on the stagnation pressure. However, the ratio of those two quantities—the missile axial specific impulse—is independent of both the stagnation and atmospheric pressures. Consequently, missile axial specific impulse is the most meaningful performance parameter for a canted scarfed propulsive nozzle.

The analysis presented herein and the preceding conclusions are based on the assumption that the nozzle pressure ratio is high enough to preclude shock waves or flow separation at the nozzle exit. Conventional nozzle flowfields can overexpand by a factor of 3-4 without separating. Very little is known about separation in a canted scarfed nozzle, where the external flowfield impinges on the nozzle plume at an angle. More studies are needed to understand this phenomenon.

Numerical Results

An extensive parametric study was conducted to investigate the performance of scarfed propulsive nozzles. The nozzle geometric parameters are illustrated in Fig. 2. In all cases, the basic nozzle was conical with normalized values of $y_t = 1.0$, $\rho_{tu} = 1.0$, and $\rho_{td} = 0.01$. Four values of the cone angle α of the basic nozzle were considered: 10, 15, 20, and 25 deg. Four values of the area ratio ϵ of the basic nozzle were considered: 5, 10, 20, and 50. Three values of the cone angle δ of the conical extension were investigated: 0, 5, and 10 deg. For all 48 combinations of α, ϵ, and δ, four values of the scarf angle β were considered: 15, 20, 30, and 40 deg. A total of 192 configurations were analyzed.

The gas thermodynamic model was $\gamma = 1.2$ and $R = 65$ (ft-lb)/(lbm-°R). The rocket motor operating conditions were $T_t = 5000$ °R, $P_t = 1000$ lbf/in.^{2}, and $P_a = 14.7$ lbf/in.^{2}.

The results of the parametric study, as specified by the axial specific impulse delivered to the missile $I_{sp,X}$ [see Eq. (5)], are presented in this section. Figures 5-7 present the missile axial specific impulse $I_{sp,X}$ as a function of the scarfed nozzle geometric parameters α, ϵ, δ, and β.

Figure 5 presents the missile axial specific impulse as a function of the expansion ratio ϵ of the basic nozzle for a cylin-

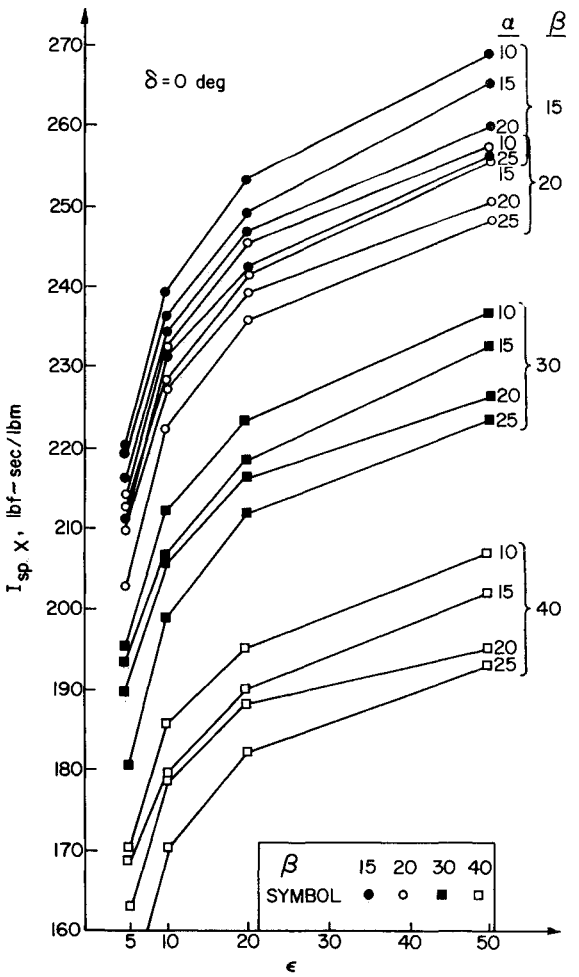

Fig. 5 Specific impulse as a function of area ratio for $\delta = 0$ deg.

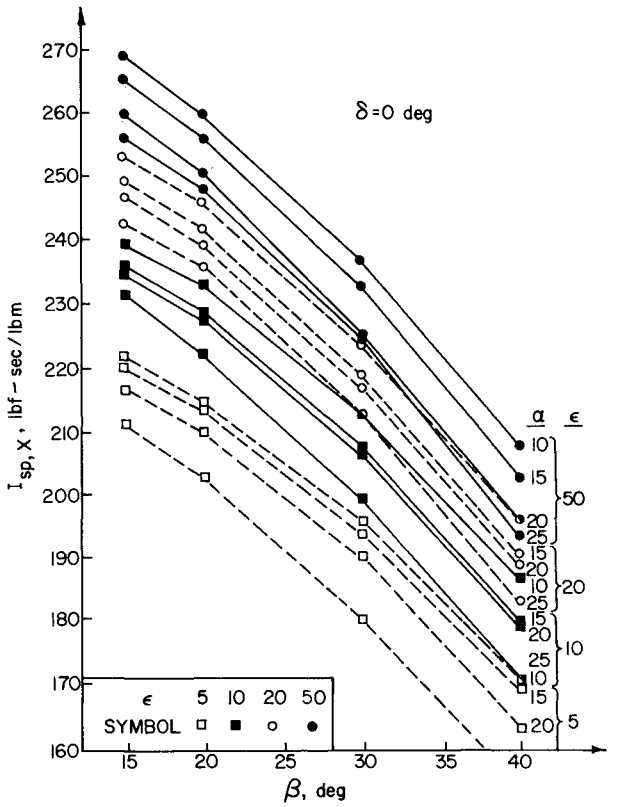

Fig. 6 Specific impulse as a function of scarf angle for $\delta = 0$ deg.

drical extension (i.e., $\delta = 0$ deg) with the nozzle cone angle α and nozzle scarf angle β as parameters. In all cases, the specific impulse increases significantly as the expansion ratio increases. There is no maximum in the curves as there is for conventional nozzles, since missile axial specific impulse is independent of atmospheric pressure. The scarf angle β is also the nozzle cant angle. As the cant angle decreases, a larger portion of the nozzle axial thrust acts along the missile axis, and the missile axial specific impule increases, as illustrated in Fig. 5. The cone angle α of the nozzle has only a minor influence on missile axial specific impulse. As the cone angle α increases, the flow turning angle across the oblique shock wave increases, thus increasing the loss in stagnation pressure and thrust. In addition, increases in the cone angle α increase the flow divergence losses in the nozzle. Both of these effects, while rather minor, cause decreases in the missile axial specific impulse as the cone angle α increases. The same trends are obtained for extension angles δ of 5 and 10 deg, although the overall performance level increases several percent as δ increases.

Figure 6 presents the missile axial specific impulse as a function of the scarf angle β for a cylindrical extension with α and ϵ as parameters. The data presented are the same as in Fig. 5, rearranged to illustrate more clearly the influence of the scarf angle β. The specific impulse decreases significantly as the scarf angle β increases.

Figure 7 presents the missile axial specific impulse as a function of the area ratio ϵ of the nozzle for the scarf angle $\beta = 30$ deg, two extension angles $\delta = 0$ and 10 deg, with the cone angle α as a parameter. The curves for $\delta = 0$ deg are the same as those in Fig. 5 for $\beta = 30$ deg. The curves for $\delta = 10$ deg show a slight increase in missile axial specific impulse as the extension angle δ increases. The major result of increasing δ is to increase the overall area ratio of the complete nozzle, which increases the internal expansion just as increasing the area ratio ϵ of the basic nozzle increases the internal expansion. Increasing δ also increases the flow divergence losses slightly, but, for δ in the range of 0-10 deg, this effect is very small. Increasing the cone angle α of the nozzle decreases the specific impulse slightly due to increasing flow divergence effects.

The parametric study presented in Figs. 5-7 presents a thorough picture of the effect of nozzle scarfing on the axial specific impulse delivered to a missile. From those results, the following general observations can be made: motor axial specific impulse 1) decreases slightly as the cone angle α of the basic nozzle increases, 2) increases significantly as the area ratio ϵ of the basic nozzle increases, 3) increases slightly as the cone angle δ of the nozzle extension increases, and 4) decreases significantly as the nozzle scarf angle (i.e., the cant angle) β increases.

Experimental Results and Discussion

The results of several series of experimental programs have been analyzed to investigate the performance of scarfed propulsive nozzles. Those results are employed to verify the performance prediction model developed during the present investigation. All of the propellants in these tests had only small amounts of aluminum, therefore, the assumption of clean gas flow is valid.

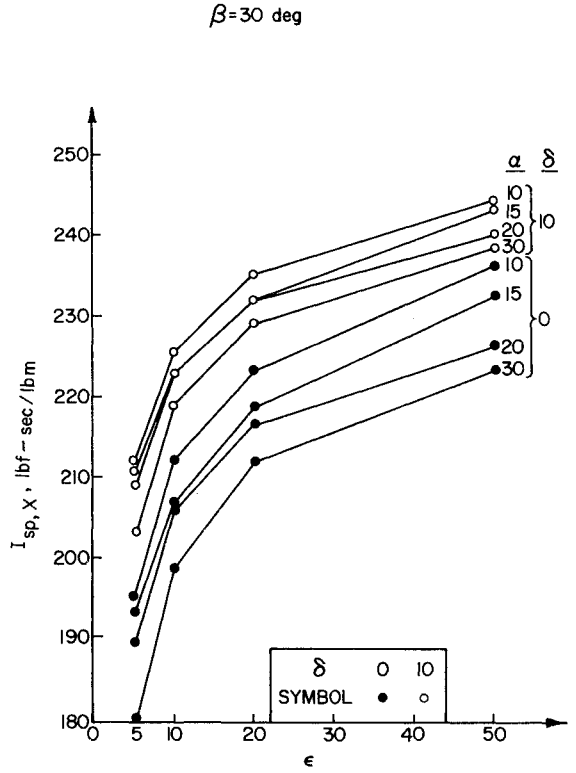

Fig. 7 Specific impulse as a function of area ratio for $\beta = 30$ deg.

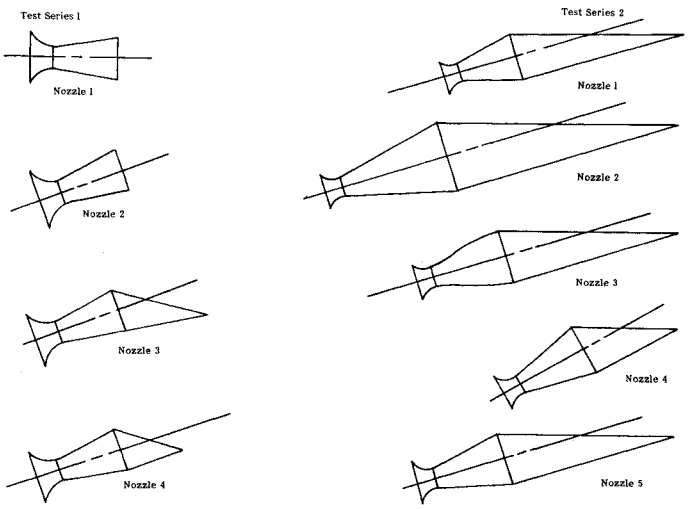

Fig. 8 Nozzle configurations for test series 1 and 2.

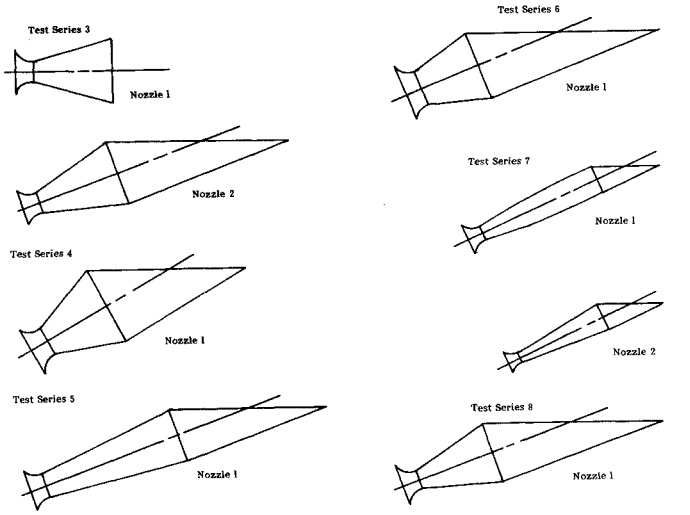

Fig. 9 Nozzle configurations for test series 3-8.

Experimental Program

Data were obtained from a total of eight different series of tests during which 45 separate rocket motor firings were made involving 17 different nozzle configurations. These tests covered a wide variety of nozzle geometries and a wide range of rocket motor operating conditions. The nozzle configurations employed are illustrated in Figs. 8 and 9. The geometric specifications of each configuration are presented in Table 1, along with the range of chamber pressures tested for each motor.

For each rocket motor firing, pressure- and thrust-time histories were measured. All of the measured thrust values are motor axial thrust. Thus, at any specific time during the course of a firing, a pressure-thrust data point can be obtained. For each motor firing, a series of pressure-thrust data points was generated. The pressure values obtained from the motor firing were used as input to the two-dimensional performance prediction program. The geometric inputs were obtained from the actual nozzle geometries. The geometric inputs reflected values obtained from physical measurements of the nozzles, including any throat erosion that may have occurred over the course of the firing. Thermodynamic inputs to the program, in particular, the specific heat ratio γ, gas constant R, and flame temperature T_f, were obtained by employing the NASA One-Dimensional Equilibrium (ODE) program.[4] These data were computed for each propellant formulation at every pressure level considered.

Nozzle Efficiency

The two-dimensional performance prediction model described in the preceding sections was applied for all of the data points. These runs produced a predicted value of thrust for each pressure value specified. Thus, for each experimental data point, a direct comparison can be made between the measured F_{meas} and predicted F_{pred} thrust. The comparison can be expressed conveniently in terms of the scarfing efficiency η_s defined as

$$\eta_S = F_{meas}/F_{pred} \tag{6}$$

However, a direct comparison of the predicted and measured thrust is not consistent, since the actual rocket motor nozzle has several thermodynamic and fluid dynamic losses that are not modeled by the scarfed nozzle performance prediction model. These losses include heat transfer to the nozzle wall, boundary-layer drag, finite-rate-kinetics effects, and two-phase flow effects. Consequently, F_{pred} will be too large since it does not include those losses, and η_s will be too low since F_{meas} includes losses other than nozzle scarfing losses. Thus, a true comparison between the predicted and

Table 1 Nozzle configurations tested

Test series No.	Motor No.	Chamber pressure range, psia	Nozzle No.	α, deg	δ, deg	β, deg	θ, deg	ϵ
	1	1504-1826	1	10	–	–	0	3.9
	2	1461-1806	2	10	–	–	20	3.8
1	3	1476-1812	3	10	10	35	20	3.9
	4	1544-1896	3					3.9
	5	1469-1807	4	10	0	35	20	3.9
	6	1470-1823	4					3.8
	1	1555-2168	1	12.73	0	16.5	16.5	6.5
	2	1559-2181	2	12.77	0	16.5	16.5	15.1
2	3	1439-1903	3	Contour	0	16.5	16.5	9.0
	4	1591-2110	4	13.44	0	30	30	9.0
	5	1443-2074	5	12.77	0	16.5	16.5	9.0
	1	1077-1253	1	15	–	–	0	8.9
	2	727-1441	1					8.9
3	3	800-1324	1					8.9
	4	889-1327	2	15	0	20	20	8.6
	5	659-1512	2					8.9
	6	1026-1248	2					8.6
4	1-13	1626-2342	1	20.17	0	30	30	7.8
5	1	256-440	1	6		20	20	4.6
	2	367-458	1					4.6
	1	131-290	1	16	0	20	20	4.7
6	2	369-441	1					4.7
	3	447-529	1					4.7
	1	202-746	1	Contour	0	25	25	7.9
7	2	306-850	1					7.9
	3	335-865	2	5	0	25	25	6.4
	4	222-680	2					6.0
	1	321-1166	1	15	0	20	20	8.8
	2	217-1228	1					10.2
8	3	194-1448	1					11.0
	4	193-1483	1					10.9
	5	625-1248	1					11.8
	6	620-1581	1					13.0

measured effects of nozzle scarfing on motor axial thrust can be made only if the other nozzle losses are accounted for.

Conventional losses in a rocket motor nozzle are accounted for by the thrust efficiency η, defined as

$$\eta = F_{\text{meas}}/F_{\text{ODE}} \tag{7}$$

where F_{ODE} is the reference ideal thrust for an isentropic equilibrium expansion calculated by the NASA ODE program.[4] The Solid Performance Program (SPP)[5] methodology can be employed to calculate this efficiency. If the efficiency η is known for a given nozzle, then any remaining difference between the performance predicted by the present scarfed nozzle performance prediction program and the measured performance can be attributed to the effects of nozzle scarfing.

The calculation of the nozzle efficiency η for the 45 rocket motor firings considered in this study was beyond the scope of the present investigation. The measured thrust was simply compared to the thrust predicted by the present methodology, and the difference was attributed to the nozzle losses accounted for in the conventional efficiency η. If the values of η obtained in this manner are reasonable for the motors being considered, then the present analysis must be modeling the scarfing effects in a reasonable manner. This procedure is somewhat indirect, but it does permit a reasonable assessment of the present scarfed nozzle performance prediction methodology.

In each test series several motor firings were conducted. For each motor firing, several pressure-thrust data points were determined. Using these experimental and predicted thrust values, a least-squares curve fit of Eq. (6) was performed for each motor firing. The results of all motor firings for a given nozzle configuration were combined to yield a curve fit for each nozzle configuration. The least-squares curve fit resulted in the following equation for the thrust efficiency:

$$\eta = \sum_{i=1}^{N} F_{\text{pred},\,i} F_{\text{meas},\,i} \Big/ \sum_{i=1}^{N} (F_{\text{pred},\,i})^2 \tag{8}$$

where $F_{\text{pred},\,i}$ is the predicted thrust value, $F_{\text{meas},\,i}$ the corresponding measured thrust value, and N the number of data points. The correlation coefficient R^2 was computed by the following equation:

$$R^2 = \left[\sum_{i=1}^{N} (F_{\text{meas},\,i} - \bar{F}_{\text{meas}})^2 - \sum_{i=1}^{N} (F_{\text{meas},i} - \eta F_{\text{pred},i})^2 \right] \div \sum_{i=1}^{N} (F_{\text{meas},\,i} - \bar{F}_{\text{meas}})^2 \tag{9}$$

where

$$\bar{F}_{\text{meas}} = \frac{1}{N} \sum_{i=1}^{N} F_{\text{meas},\,i} \tag{10}$$

Least-squares curve fits were performed for each nozzle configuration and each motor firing for seven of the eight test series. The results of these curve fits are presented in Table 2. The individual data points for each motor firing for test series 1 are presented in Fig. 10. Corresponding figures for test series 2-8 are presented in Ref. 1. The curve fits for each nozzle configuration are also presented in these plots.

The results of the curve fits must be interpreted in view of the objectives of each test series. Test series 1-3 were conducted specifically to investigate the performance of scarfed nozzles. The remaining test series simply involved the testing of rocket motors employing scarfed nozzles. Those test series were not designed specifically for scarfed nozzle performance evaluations. Thus, emphasis is placed on the results of test series 1-3.

Test Series 1

Test series 1 involved the testing of four nozzle configurations. The objective of test series 1 was to experimentally determine the effects of cant angle, the conical scarfed section, and the cylindrical extension. Nozzle 1 is a conventional conical nozzle, nozzle 2 a canted conventional conical nozzle, and nozzle 3 a canted scarfed conical nozzle. Nozzle 4 is a canted conical nozzle with a scarfed cylindrical extension, with the scarf angle greater than the cant angle. In all four nozzles, the initial conical section is identical. The flowfield in nozzles 1 and 2 is completely axisymmetric with no shock waves. The degree of confidence in the ability of the two-dimensional model to predict the performance of such nozzles is very high, thus, the thrust efficiency obtained for these nozzles should be very reliable. Therefore, if the scarfed nozzles have the same thrust efficiencies as the nonscarfed nozzles, the effects of scarfing will have been accounted for and the performance prediction model will have been verified.

The comparison of the measured and predicted thrusts for test series 1 is presented in Fig. 10. From Table 2, the curve fits for the nozzle efficiencies yield the following results: for nozzles 1, 2, 3, and 4, $\eta = 95.7$, 95.2, 94.8, and 92.4%, respectively.

These result show good correlation between the predicted and measured performance for nozzles 1-3. However, the performance of nozzle 4 is overpredicted even when the various losses are taken into account.

Test Series 2

In test series 2, all of the nozzles considered were scarfed. The purpose of this test series was to investigate the effects of cant angle, expansion ratio, and the contour of the nonscarfed section of the nozzle. The effect of the nonscarfed contour was investigated in nozzle 3, in which the basic nozzle had a continuously turning contour that attached smoothly to the cylindrical extension. From Table 2, the curve fits of the nozzle efficiencies yield: for nozzles 1, 2, 3, 4, and 5, $\eta = 93.8$, 92.8, 91.4, 94.5, and 95.4%, respectively.

These results are in reasonable agreement, except for nozzle 3, thus indicating that the code is modeling the effects of nozzle scarfing correctly. The performance of nozzle 3 is overpredicted even when thermodynamic losses are accounted for. The basic nozzle contour for nozzle 3 is a continuously turning contour that attaches tangentially to the cylindrical scarfed extension. The performance prediction code models this flowfield with no discrete shock waves. However, there is

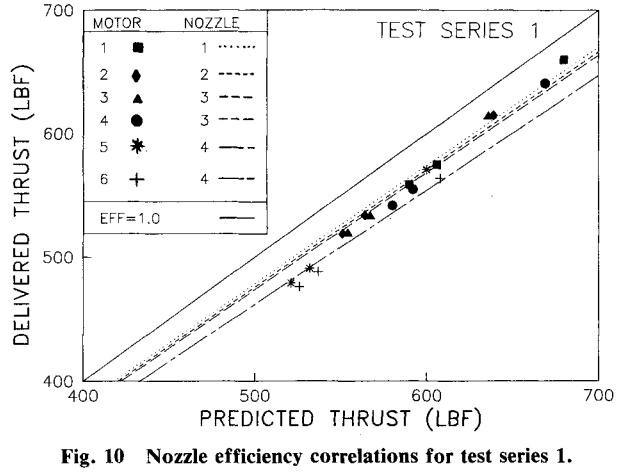

Fig. 10 Nozzle efficiency correlations for test series 1.

Table 2 Results of correlation analysis

Motor data correlations					Nozzle data correlations				
Test series No.	Motor No.	No. of data points	η	R^2	Nozzle No.	No. of motor firings	No. of data points	η	R^2
	1	3	0.9570	0.9760	1	1	3	0.9750	0.9760
	2	3	0.9516	0.9843	2	1	3	0.9516	0.9843
1	3	3	0.9507	0.9663	3	2	6	0.9476	0.9721
	4	3	0.9448	0.9768					
	5	3	0.9332	0.9591	4	2	6	0.9240	0.9526
	6	3	0.9151	0.9784					
	1	3	0.9377	0.9998	1	1	3	0.9377	0.9998
	2	3	0.9277	0.9913	2	1	3	0.9277	0.9913
2	3	3	0.9139	0.9958	3	1	3	0.9139	0.9958
	4	3	0.9445	0.9980	4	1	3	0.9445	0.9980
	5	3	0.9542	0.9999	5	1	3	0.9542	0.9999
	1	10	0.9372	0.9717	1	3	26	0.9645	0.9520
	2	11	1.0011	0.9912					
3	3	5	0.9406	0.9996					
	4	11	0.9266	0.9813	2	3	26	0.9472	0.9748
	5	11	0.9702	0.9993					
	6	4	0.9360	0.9984					
4	1-13	2	–	–	1	13	26	0.9258	0.9492
5	1	11	1.0268	0.8408	1	2	20	1.0007	0.7924
	2	9	0.9746	0.9445					
	1	11	0.8549	0.9468	1	3	25	0.9187	0.9877
6	2	7	0.9219	0.9221					
	3	7	0.9379	0.9500					
	1	25	0.9002	0.9868	1	2	48	0.9377	0.9650
7	2	23	0.9671	0.9621					
	3	25	0.9289	0.9773	2	2	51	0.9242	0.9876
	4	26	0.9164	0.9858					
	1	14	0.9634	0.9945	1	6	134	0.9434	0.9555
	2	23	0.9353	0.9851					
8	3	23	0.9239	0.9970					
	4	23	0.9142	0.9950					
	5	26	0.9027	0.9403					
	6	25	1.0344	0.9623					

probably an embedded shock wave in the basic nozzle. This shock wave will result in a performance loss not accounted for by the present model, thus accounting for the overprediction of the performance of nozzle 3.

Test Series 3

In test series 3, the effect of cant angle and the addition of a cylindrical scarfed section were investigated. Nozzle 1 is a conventional axisymmetric nozzle. Nozzle 2 is a scarfed nozzle with a cylindrical scarfed section. From Table 2, the curve fits of the nozzle efficiencies yield: for nozzles 1 and 2, $\eta = 96.5$ and 94.7%, respectively.

These results show good agreement between the efficiencies for the two configurations, indicating a good correlation between the predicted and measured effects of nozzle scarfing.

Test Series 4-8

Test series 4-8 all involved tests of rocket motors employing scarfed nozzles. However, with the exception of test series 7, these motor firings involved a single nozzle configuration. None of these tests were specifically intended to measure scarfed nozzle performance effects, thus, cannot be used to determine the ability of the model to predict the influence of various factors on scarfed nozzle performance. However, these tests did indicate a general agreement between the predicted and measured effects of nozzle scarfing. The comparisons of the predicted and measured thrusts for these test series are presented in Ref. 1.

Conclusions

An analysis, and a computer program based on that analysis, have been developed for predicting the performance of side-exhausting scarfed propulsive nozzles. The results of an extensive parametric study illustrated the dependence of motor axial specific impulse on nozzle cone angle, area ratio, extension angle and scarf angle. The specific impulse decreases slightly as cone angle increases, increases significantly as the area ratio increases, increases slightly as the nozzle extension angle increases, and decreases significantly as the nozzle scarf angle (cant angle) increases. Comparison with the results of several experimental programs demonstrated the validity of the analysis. The present analysis gives the nozzle designer an accurate tool for predicting the performance of side-exhausting scarfed propulsive nozzles.

Acknowledgments

The initial inspiration for this work came from Mr. A.R. Maykut of the Propulsion Directorate, U.S. Army Missile Command. His guidance, counsel, and assistance were invaluable to the program. The experimental results were obtained from a wide variety of sources. Mr. Bryon Cockrell of Atlantic Research Corporation provided motor firing data and engineering drawings. Mr. Donald Sine of Hercules Inc. provided detailed motor performance data and nozzle geometry data. Messrs. Ben Wilson and James Hodges of the Propulsion Directorate, U.S. Army Missile Command, provided performance data and engineering drawings for several programs. Mr. Francis Thiessen of the Propulsion Directorate provided additional engineering drawings. The support and assistance of all of these people contributed greatly to this investigation.

References

[1]Lilley, J.S. and Hoffman, J.D., "Performance Analysis of Scarfed Nozzles," AIAA Paper 84-1416, June 1984.

[2]Kliegel, J.R. and Levine, J.N., "Transonic Flow in Small Throat Radius of Curvature Nozzles," *AIAA Journal,* Vol. 7, July 1969, pp. 1375-1378.

[3]Zucrow, M.J. and Hoffman, J.D., *Gas Dynamics,* Vols. 1 and 2, John Wiley & Sons, New York, 1976.

[4]Gordon, S. and McBride, B.J., "Computer Program for Calculation of Complex Chemical Equilibrium Compositions, Rocket Performance, Incident and Reflected Shocks, and Chapman-Jouguet Detonations," NASA SP-273, 1971.

[5]Nickerson, G.R., Coates, D.E., and Hermsen, R.W., "A Computer Program for the Prediction of Solid Propellant Rocket Motor Performance," AFRPL-TR-80-34, Vols. 1-III, April 1981.

From the AIAA Progress in Astronautics and Aeronautics Series...

ENTRY HEATING AND THERMAL PROTECTION—v. 69

HEAT TRANSFER, THERMAL CONTROL, AND HEAT PIPES—v. 70

Edited by Walter B. Olstad, NASA Headquarters

The era of space exploration and utilization that we are witnessing today could not have become reality without a host of evolutionary and even revolutionary advances in many technical areas. Thermophysics is certainly no exception. In fact, the interdisciplinary field of thermophysics plays a significant role in the life cycle of all space missions from launch, through operation in the space environment, to entry into the atmosphere of Earth or one of Earth's planetary neighbors. Thermal control has been and remains a prime design concern for all spacecraft. Although many noteworthy advances in thermal control technology can be cited, such as advanced thermal coatings, louvered space radiators, low-temperature phase-change material packages, heat pipes and thermal diodes, and computational thermal analysis techniques, new and more challenging problems continue to arise. The prospects are for increased, not diminished, demands on the skill and ingenuity of the thermal control engineer and for continued advancement in those fundamental discipline areas upon which he relies. It is hoped that these volumes will be useful references for those working in these fields who may wish to bring themselves up-to-date in the applications to spacecraft and a guide and inspiration to those who, in the future, will be faced with new and, as yet, unknown design challenges.

Published in 1980, Volume 69—361 pp., 6×9, illus., $25.00 Mem., $45.00 List
Published in 1980, Volume 70—393 pp., 6×9, illus., $25.00 Mem., $45.00 List

TO ORDER WRITE: Publications Dept., AIAA, 1633 Broadway, New York, N.Y. 10019